AD-A148 557 CONTINUED STUDIES IN HALL CURRENT EFFECTS ON BEAM STABILITY(U) SCIENCE APPLICATIONS INC PALO ALTO CA R L FEINSTEIN ET AL. 31 OCT 83 SAI-U-66-PA 1/1

UNCLASSIFIED AFOSR-TR-84-1076 F49620-81-C-0012 F/G 20/3 NL

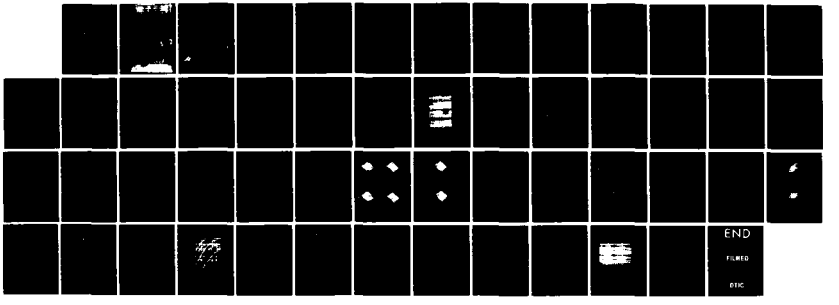

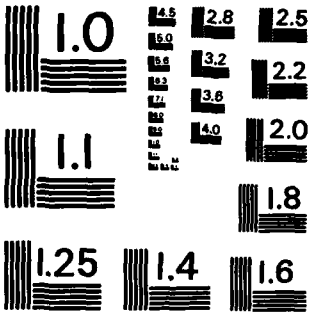

MICROCOPY RESOLUTION TEST CHART
NATIONAL BUREAU OF STANDARDS-1963-A

AD-A148 557

CONTINUED STUDIES IN HALL CURRENT EFFECTS ON BEAM STABILITY

2

SAI-U-66-PA

CONTINUED STUDIES IN HALL CURRENT EFFECTS ON BEAM STABILITY

D.A. Keeley
R.L. Feinstein

31 October 1983

Annual Technical Report

prepared for
Air Force Office of Scientific Research
Bolling Air Force Base
Washington, D.C. 20332

under contract
F49620-81-C-0012

SCIENCE APPLICATIONS INTERNATIONAL CORP.
5150 EL CAMINO REAL
SUITE B-31
LOS ALTOS, CA 94022

UNCLASSIFIED

SECURITY CLASSIFICATION OF THIS PAGE *(When Data Entered)*

REPORT DOCUMENTATION PAGE	READ INSTRUCTIONS BEFORE COMPLETING FORM
1. REPORT NUMBER: 17 M 2. GOVT ACCESSION NO.: AD-A148 537	3. RECIPIENT'S CATALOG NUMBER
4. TITLE *(and Subtitle)*: Continued Studies in Hall Current Effects on Beam Stability	5. TYPE OF REPORT & PERIOD COVERED: Annual Technical Report 17 MAR 82 - 31 OCT 83
	6. PERFORMING ORG. REPORT NUMBER: SAI-U-66-PA
7. AUTHOR(s): R.L. Feinstein, D.A. Keeley	8. CONTRACT OR GRANT NUMBER(s): F49620-81-C-0012
9. PERFORMING ORGANIZATION NAME AND ADDRESS: SCIENCE APPLICATIONS, INC. 5 Palo Alto Square, Suite 200 Palo Alto, CA 94306	10. PROGRAM ELEMENT, PROJECT, TASK AREA & WORK UNIT NUMBERS: 0002AC 63605F
11. CONTROLLING OFFICE NAME AND ADDRESS: AFOSR/NP Building 410 Bolling AFB, Ohio 20332	12. REPORT DATE: 31 October 1983 13. NUMBER OF PAGES: 46
14. MONITORING AGENCY NAME & ADDRESS *(if different from Controlling Office)*	15. SECURITY CLASS. *(of this report)*: UNCLASSIFIED 15a. DECLASSIFICATION/DOWNGRADING SCHEDULE
16. DISTRIBUTION STATEMENT *(of this Report)*	
17. DISTRIBUTION STATEMENT *(of the abstract entered in Block 20, if different from Report)*	
18. SUPPLEMENTARY NOTES	
19. KEY WORDS *(Continue on reverse side if necessary and identify by block number)*: Hall currents High current beams Hose HERMES Low density conductivity	
20. ABSTRACT *(Continue on reverse side if necessary and identify by block number)*: Two topics are discussed in this report: (1) application of a non-local conductivity model to high current beams, and (2) hose growth calculations for HERMES. Hall currents and non-ohmic effects are found to be very significant at densities $\rho/\rho_0 \lesssim .01$. Hose growth saturation for HERMES is predicted at a level which should be testable in experiments.	

DD FORM 1 JAN 73 1473 EDITION OF 1 NOV 65 IS OBSOLETE

SECURITY CLASSIFICATION OF THIS PAGE *(When Data Entered)*

TABLE OF CONTENTS

LIST OF ILLUSTRATIONS

List of Figures Continued

LIST OF TABLES

1.0 INTRODUCTION

This report summarizes recent progress by Science Applications, Inc., (SAI) in the investigation of low-density air chemistry and tensor conductivity (Hall-current effects) and its impact on high-current beam stability.

In Section 2.0, the results of modeling high current beams in low-density air are discussed. At low-densities, the standard simplifying assumptions usually employed in conductivity modeling no longer apply: scalar conductivity, ohm's law; local-instantaneous energy deposition; Maxwellian distributed plasma electrons; no delta rays; and no inertial effects. These assumptions are not made in the present model. It is concluded that Hall currents do play a significant role at low enough densities and that the redistribution of plasma current can result in a significant but sudden increase in the magnetic pinch below a "critical" air density.

In Section 3.0 we discuss the viability of using the AFWL/SNLA HERMES facility for addressing important issues of high-current hose stability. It is concluded that with proper pulse conditioning, the HERMES pulse should be able to test high-current hose growth saturation and calibrate existing hose codes.

2.0 HIGH CURRENT BEAMS IN LOW DENSITY AIR

2.1 Introduction

We report here the first results of applying a phenomenological low-density chemistry code to high current beams. A brief account of the model has been given previously (Refs. 1 and 2). However, substantial modifications were necessary for application to high current beams. The model is not considered complete, and there are no independent calculations in the same parameter regime to which it can be compared; thus the quantitative results are tentative.

Conclusions based on the calculations are:

1) Below a certain model-dependent density $\sim .01$ normal, the electric field drives a bulk runaway which changes the distribution of plasma currents. The net result is a sudden significant increase in the pinch force as the density is decreased below the critical value.

2) If Hall currents are turned off, the enhanced pinch may be reduced by as much as a factor of two at one Bennett radius.

3) Significant amounts of plasma current are driven by the gradient in electron pressure.

4) Significant amounts of plasma current are carried by the high-energy non-Maxwellian part of the electron distribution.

This section is divided into three main topics: (1) a discussion of the physics requirements for low-density calculations, (2) an outline of the present status of the model, and (3) a discussion of the computational results for high current beams.

2.2 Beam-Driven Chemistry in the Low-Density Regime

Simple order-of-magnitude argments show that at background densities sufficiently lower than normal atmospheric density, several key assumptions built into standard beam chemistry codes are not justified. Among these inapplicable assumptions are:

1) The beam-initiated cascade results in local, instantaneous production of electrons and ions.

2) Currents associated with the cascade itself can be neglected.

3) Plasma currents can be calculated from Ohm's law.

4) The electron and ion densities are always almost equal, so transport effects can be ignored in the chemistry calculations.

5) The electron distribution remains close to Maxwellian, so that the high energy parts of the distribution are no more important than usual in determining currents, ionization rates, etc.

In addition, many beam chemistry codes use electromagnetic algorithms which ignore Hall current effects. This assumption can break down in two ways at low density: (a) the momentum transfer frequency goes down with the density, so that it may not exceed the Larmor frequency by a wide margin as in full-density air, and (b) the highly-overpopulated high energy tail of the electron distribution at low density may have a momentum transfer frequency considerably lower than that of the bulk of electrons, and thus make a larger contribution to the current.

In the past (Ref. 3) we have investigated the effects of Hall currents in full and reduced density air, but have not been able to address problem (b) above. In addition, we have made assumptions 1 - 5 in our chemistry codes. At present we are developing for DARPA a multi-energy-group model which abandons assumptions 1 - 5 and addresses the non-Maxwellian aspects of Hall current calculations. Recent calculations by Yu (Ref. 4) have confirmed the importance of Hall current effects for ATA-like beams when the electron energy distribution is treated in detail. The present work verifies their importance for high current beams.

2.3 Non-Local, Non-Ohmic Conductivity Model

The ultimate goal of the development program is to produce a relatively simple BMCOND-like model which can be incorporated into propagation codes. This requirement eliminates the possibility of doing a "first principles" calculation. The approach taken is to develop a phenomenological model which represents the most important physical processes in a simple way, and to adjust the "free" parameters associated with various simplifying assumptions to obtain agreement with more fundamentally-based calculations.

The model described below considers the electron distribution broken into three energy ranges. The lowest energy group represents basically the usual bulk of approximately-Maxwellian electrons. The next higher energy group represents those that in the presence of an electric field, are in the runaway regime and thus behave very differently from the bulk of the electrons. The third group represents the relativistic particles produced directly by the beam.

The organization of the model is summarized in Fig. 1, in which the sources and sinks of particles for each group are shown schematically. The three energy ranges will be referred to by the names low-group, high-group, and δ-group in order of increasing energy. The beam particles themselves constitute a fourth group which is treated in the usual way (e.g., no energy straggling).

The beam particles collisionally produce secondaries directly in each of the three groups, according to a Moller distribution (modified at low energy). The maximum δ-ray energy is one-half the beam energy, since the higher energy particle emerging from a primary interaction remains associated with the beam. Collisions by beam particles are the only source of electrons in the δ-group. A more detailed discussion of the δ-ray model is given below in Section 2.3.1.

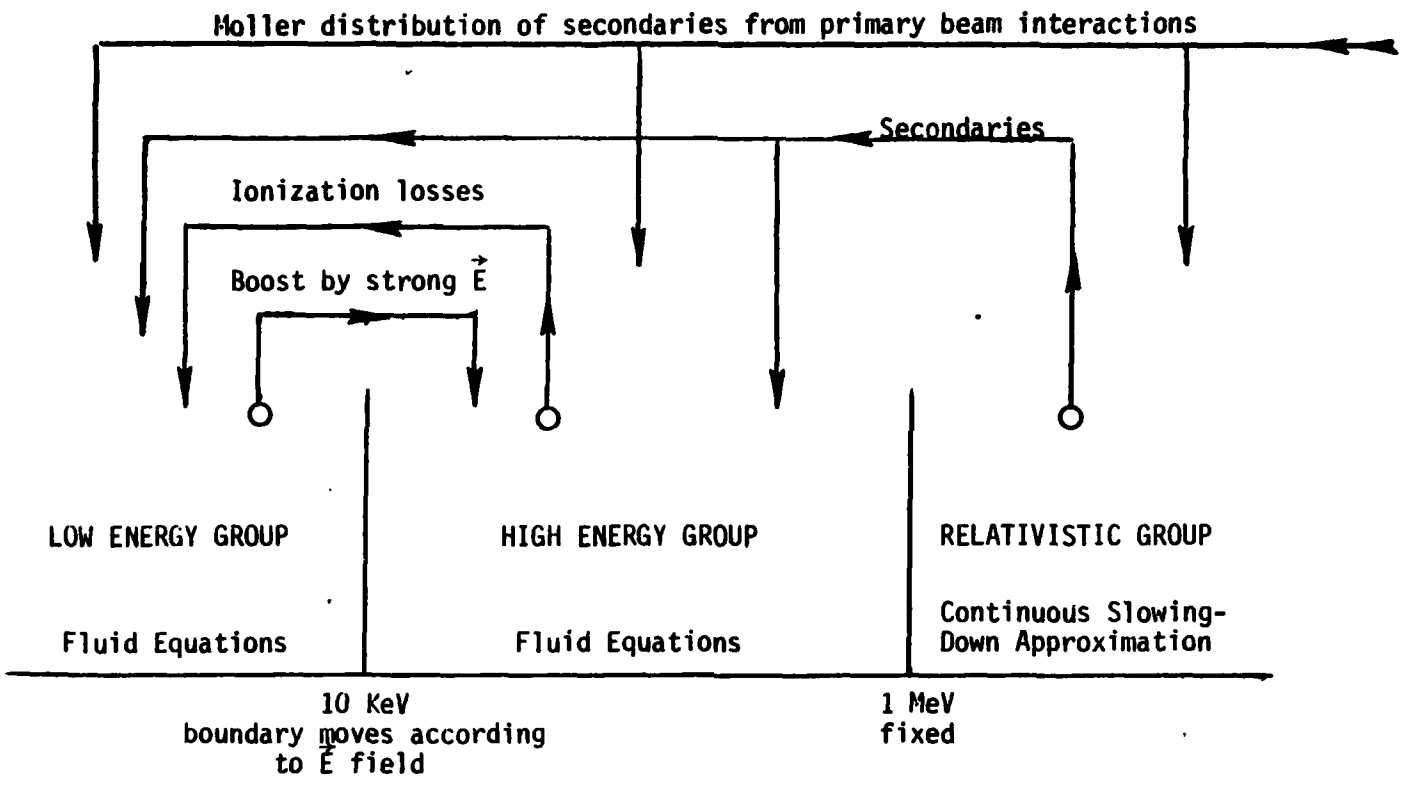

Figure 2.1. 3-Group Model.

The high-energy group extends downward from 1 MeV to a variable-energy boundary which at present goes no higher than 10 KeV. It is fed mainly by primary beam collisions, and by the collisional degradation of the δ-group through its 1 MeV lower boundary. Under some conditions, electrons are also transferred up from the low group.

Both the high and low energy electron groups are represented by fluid equations for particle density, momentum and energy. The equations of motion provide the means for abandoning the ohmic representation of plasma current flow. The fluid equations are solved on an Eulerian grid which is the same grid used for the electromagnetic field calculation. It is assumed that everything is a function of the "retarded" time variable $\xi \equiv t - z/c$ only, so that the only independent variables are r, the radial position, and ξ, the distance back from the pulse head in seconds. The electromagnetic fields are obtained using the algorithm described in Ref. 3.

In principle it is necessary to solve the fluid equations and δ-group equations simultaneously with the electromagnetic field equations. Since the Maxwell equations themselves are explicitly non-linear when the Hall current terms are included, and the fluid equations are also non-linear, an iterative procedure is required. In order to maintain maximum modularity under these circumstances, the procedure adopted involved solving first a linearized set of fluid equations, followed by the field equations, and then iterating to convergence.

In addition, the algorithm has been designed to allow differential comparisons between the three-group model, and a model with the high energy and δ-groups eliminated and with the standard local-instantaneous approximations made. However, this latter "one-group model" still differs from standard chemistry codes in that it solves an equation of motion for the one group rather than using Ohm's law. It is also possible to turn off the pressure terms in the equations of motion, and the Hall current effects.

2.3.1 Delta-Ray Group

In the present discussion, δ-rays will refer to the part of the beam-initiated cascade which has energy greater than 1 MeV. These particles are represented by a model essentially identical to that developed by Johnston (Ref. 5). As applied here, the model has two main deficiencies: (1) it does not provide detailed information on the radial distribution and (2) it does not include the effects of electric or magnetic fields on the δ-particles. With the assumption that everything depends on $\xi \equiv t - z/c$, the model gives an integral expression for the total δ-ray current as a function of distance ξ back from the beam head. Particle energy distribution information is available but not used at present.

It is assumed that most of the particles produced as secondaries by the δ-rays have very low energy. This is consistent with the continuous slowing down approximation which forms the basis of the model. In the present model, as the δ-rays lose energy, they produce low energy electrons at a rate of one particle per 33.73 eV of energy lost; these particles immediately enter the low-energy plasma electron group of the three-group model. The δ-rays themselves degrade in energy due to collisions. They reach the cutoff of 1 MeV at a rate given by the Johnston model, and at this point they are added to the high energy electron group.

The radial profile as a function of distance back from the beam head is estimated in a crude way, based on two pieces of information: (1) the δ's are produced with the beam profile and (2) they evolve from that profile to form a halo with radial dimension estimated by Johnston (Ref. 5) to be ~ 4 Bennett radii about a Bennett-profile beam (for particles above 1 MeV). It is assumed that at a given ξ, the profile towards which the δ's evolve is a weighted average of the beam profile and a specified halo profile. The relative weights are determined from the rate of local production as compared to the total instantaneous number density, and the rate of evolution towards the halo profile. This assumption is used in the following interpolation formula for the radial profile $f(r, \xi+\Delta\xi)$ in terms of $f(r,\xi)$:

$$f(r, \xi+\Delta\xi) = (f(r,\xi) + \Delta\xi F)/(1 + \nu_d \Delta\xi).$$

The function F is given by

$$F = (\frac{S}{N} h + g \nu),$$

where S is the local rate of δ-ray production by the beam, N is the total number of δ-rays present, and h is the beam profile, on which the δ-rays are produced. The profile g is the assumed halo profile, and ν is a characteristic rate at which the δ's evolve towards the profile g. The rate ν_d is set equal to S/N + ν. With this choice, $f(r,\xi+\Delta\xi)$ is normalized to unity if h, g, and $f(r,\xi)$ are. The rate ν is taken to be an average radial velocity of the δ's divided by the assumed halo characteristic radius.

2.3.2 The High-Energy Group

The schematic forms of the fluid equations for the high-group are:

$$\frac{\partial N}{\partial t} + \nabla\cdot(N\vec{v}) + \nu_1 N = S_B + S_\delta + S_L \qquad (2.1)$$

$$\frac{\partial \vec{J}}{\partial t} + \nabla\cdot(\vec{J}\vec{v}) + \frac{1}{m}\nabla P + \nu_2 \vec{J} = \vec{K}_B + \vec{K}_\delta + \vec{K}_L + \frac{Ne}{m}(\vec{E} + \frac{\vec{v}}{c}\times\vec{B}) \qquad (2.2)$$

$$\frac{\partial}{\partial t}(\frac{1}{2} Nmv^2 + \frac{3}{2} P) + \nabla\cdot[\vec{v}(\frac{1}{2} Nmv^2 + \frac{3}{2} P)] + \nabla\cdot(\vec{v}P) + \nu_1(\frac{1}{2} Nmv^2 + \frac{3}{2} P) = L + Ne\vec{E}\cdot\vec{v} \qquad (2.3)$$

The terms S_B, $\vec{K}_B$, etc. are the sources due to the beam, the δ-group, and upward transfer from the low-group, respectively. It is assumed that all collisional ionizations by high-group electrons produce a low energy secondary which goes directly into the low group. The energy equation (2.3) has been written with the total energy split into a drift part, and a thermal part represented by a pressure P. The term L includes energy deposited by the beam, energy brought in by transfer of particles from the low-group and δ-group, and energy losses due to ionization. Energy loss due to loss of particles from the high group is

represented by the ν_1 term on the left side of the equation. It has been assumed that the particles lost take with them the average energy of the high group. The momentum loss rate ν_2 includes the effect of particle losses, momentum loss due to ionizing collisions, and momentum loss due to elastic collisions.

The fluid equations are solved as a finite difference system on the Eulerian electromagnetic field grid. The outer boundary condition allows an outflow of particles. No explicit assumption is made concerning the distribution function of the high group electrons except at $\xi = 0^+$, when it is dominated by the Moller distribution from primary beam particle interactions. The average total energy and z-momentum are then used to give an initial "temperature" T, defined by $P = NT$, where P is the pressure from Eq. (2.3). At all subsequent times, the temperature, particle density, and drift velocity are obtained from the fluid equations.

For simplicity, ionization and momentum transfer rates are evaluated at the mean particle energy. An analytic formula given by Briggs and Yu (Ref. 6) is used for the ionization cross section. The momentum transfer frequency ν_m is given by the approximate formula

$$\nu_m = (1.08 \times 10^{-5} N_g \mathcal{E}^{1/2})/(178.89 + \mathcal{E}^{3/2}) + (1.46 \times 10^{-6} N^+ \log \Lambda)/T_{equiv}^{3/2} \qquad (2.4)$$

where $\mathcal{E}$ is the total electron energy in volts. The first term represents the effect of collisions with neutral particles, and the second represents Coulomb collisions. The "equivalent" temperature is defined as $T_{equiv} = T + 1/3\ mv^2$, $\log \Lambda$ is the usual Coulomb logarithm, N_g is the total density of neutral atoms and molecules, and N^+ is the total density of positive ions.

The boundary between the high and low energy groups is set by finding the solution of the equation

$$e E = m \nu_m \bar{v} \qquad (2.5)$$

corresponding to the high energy side of the peak in ν_m. The average velocity $\bar{v}$ is related to the total energy $\mathcal{E}$ appearing in Eq. (2.4) by $\mathcal{E} = \frac{1}{2} m \bar{v}^2$. However, the boundary energy is not allowed to exceed 10 KeV even when the total electric field E is very small.

Another special case occurs when the field is so strong that there is no physical solution to (2.5); this corresponds to a bulk runaway, in which the field is capable of accelerating the electrons through the peak of the momentum transfer cross section. In this case, the choice of the lower boundary of the high group is somewhat arbitrary. The lower limit to be used for the boundary during a strong runaway condition can be specified as input data. Usually it is taken to be $\sim$ a few volts, so that essentially all the electrons produced directly by the beam go into the low end of the high energy group. The transfer of electrons from the low to the high group is discussed below.

2.3.3 The Low-Energy Group

The equations for the low energy group are similar in form to those given above for the high group with the exception that they contain loss terms due to recombination and to transfers to the high energy group, and input terms due to transfers from the high group and to collisional ionization by high group electrons. The main difference in the treatment of the low group is in the chemistry detail. At present, the abundance of N_2, O_2, N, $N(^2D)$, O, and a composite representative of the triplet states of N_2 are followed explicitly by differential equations. The system of equations used is essentially the same as in the chemistry code BMCOND (Ref. 8). This degree of complexity was found necessary to obtain reasonable agreement with the comprehensive code HICHEM at low air densities for high current calculations.

Ionization rates are given by tables identical to those in the HICHEM code up to 500 volts "equivalent" temperature ($T_{equiv} \equiv T_e + 1/3\ m\ v^2$). The collisional excitation rates from the BMCOND model are used. Ionization and excitation rates due to the beam are computed as in the HICHEM code, but with appropriate adjustment for the differences between time-delayed deposition model used here and the instantaneous deposition model in HICHEM and BMCOND.

It is very important to distinguish between the positive ion density and the electron density, since electron transport effects can be very large; thus a separate differential equation for the total rate of positive ion production is integrated. In addition it was found necessary to calculate a vibrational temperature because of significant sensitivity of computational results to the dissociative recombination rate; the HICHEM treatment was adopted for this calculation. The momentum transfer frequency used in BMCOND is used for low energies, with a smooth transition to the analytic formula (Eq. 2.4) used for the high group. The Coulomb term of Eq. (2.4) is used throughout.

Reassignment of electrons from the low group to the high group is a relatively arbitrary procedure. The goal is to remove electrons from a presumed high-energy non-Maxwellian tail of the low group and put them into the high group, which hopefully represents better their contribution to currents, ionization rates, etc. than does the assumed Maxwellian bulk of the low group electrons. However, there is no simple model of the super-thermal tail as generated by strong electric fields which vary rapidly in both time and space. Several different ad hoc procedures have been tried, but none is especially defensible in detail.

Qualitatively, what happens in a weak field (or high ambient density gas) is not very sensitive to the details of the transfer rate. Under strong runaway conditions, the entire low group is accelerated to high drift energy and heated to temperatures $\sim$ kilovolts on a very short timescale. During this time, the distinction between the two groups is not very meaningful, and again the behavior of the bulk plasma is not too sensitive to the details of the transfer

rate. However, after the fields which precipitate a strong runaway die out, the distribution of electrons between the two groups can be important; this does depend strongly on the transfer rate. Similarly, if conditions for a strong runaway are just barely achieved, for only a short time, there may be some sensitivity to the transfer rate. These problems are continually being studied, both in the context of the model described here, and through comparison with other, more comprehensive models being developed.

The transfer rate presently used is calculated as follows. A velocity v_0 is defined by $v_0 = \pm v_r + .5\, V_t$, where the + sign is taken if the radial drift velocity is parallel to E_r, and a negative sign is taken if it is opposed. The thermal velocity term V_t is added to account for the fact that at high enough temperature, a substantial number of electrons may be able to run away even if the bulk drift is not large (or even parallel to the E_r field). The transfer rate of electrons is then given by

$$S_L = \min(.5,\ .1N_h/N_e)\ \min(1.,\ \exp(\frac{v_0 - v_c}{V_t}))/\Delta\xi, \qquad (2.6)$$

in which v_c is the velocity corresponding to the energy boundary between the groups, N_h is the local density of high-group electrons, N_e is the local density of low-group electrons, and $\Delta\xi$ is the proposed timestep. The purpose of the first minimum function is to assure that the high-group density is not changed by more than 10% during the step. In actual computations, the transfer rate is usually very low, or else as high as permitted by the first factor of (2.6), even for exceedingly small timesteps.

The momentum transferred with the particle is taken to be parallel to its total drift velocity, with magnitude given by the larger of the velocities v_0 and v_c. The energy transferred is the average energy per particle of the low group, plus an additional amount arranged to come (by suitable terms in the equations of motion) entirely from the drift energy of the low group, to make up the total drift energy of the electron injected into the high group.

The net result is to decrease the drift energy of the low group, but leave its temperature unchanged. The effect of the energy and momentum transfers on the high group depends on its energy and momentum at the time of the transfer. Other procedures for transferring electrons to the high group are being evaluated.

2.4 Calibration in the High Current Regime

At present there are no comprehensive, first-principles calculations to provide detailed guidance in the development of the three-group model for high current calculations. Yu (Ref. 4) has presented Boltzmann-code calculations for ATA-like parameters, but even these calculations incorporate assumptions which are not always justified in the context of high power beam plasmas. The purpose of the calibration runs discussed below is to check that the relatively simple model described in Section 2.3 agrees reasonably well with detailed chemistry codes in regimes where the assumptions of those codes (see Section 2.2) are not thought to be seriously in error. Results of calibration at 10 kA have been presented elsewhere (Ref. 1). A similar comparison with the HICHEM (Ref. 7) code at 100 kA and gas density 0.1 normal is given below. The rise time is 5 ns and the Bennett radius is 0.5 cm.

The comparison of electron densities on axis and at one Bennett radius is shown in Figure 2.2. The agreement is very satisfactory. The effect on the electron density due to the time delay for the three-group model is not large after 2 or 3 ns. The electron density on axis is mainly determined by the close balance between collisional ionization and dissociative recombination after a few ns. The recombination rate itself decreases significantly as the molecules (and molecular ions) are depleted, and as the vibrational temperature increases. After about 6 ns, the continued increase in N_e is determined mainly by the decrease in the recombination rate, with a large part attributable to the vibrational temperature dependence.

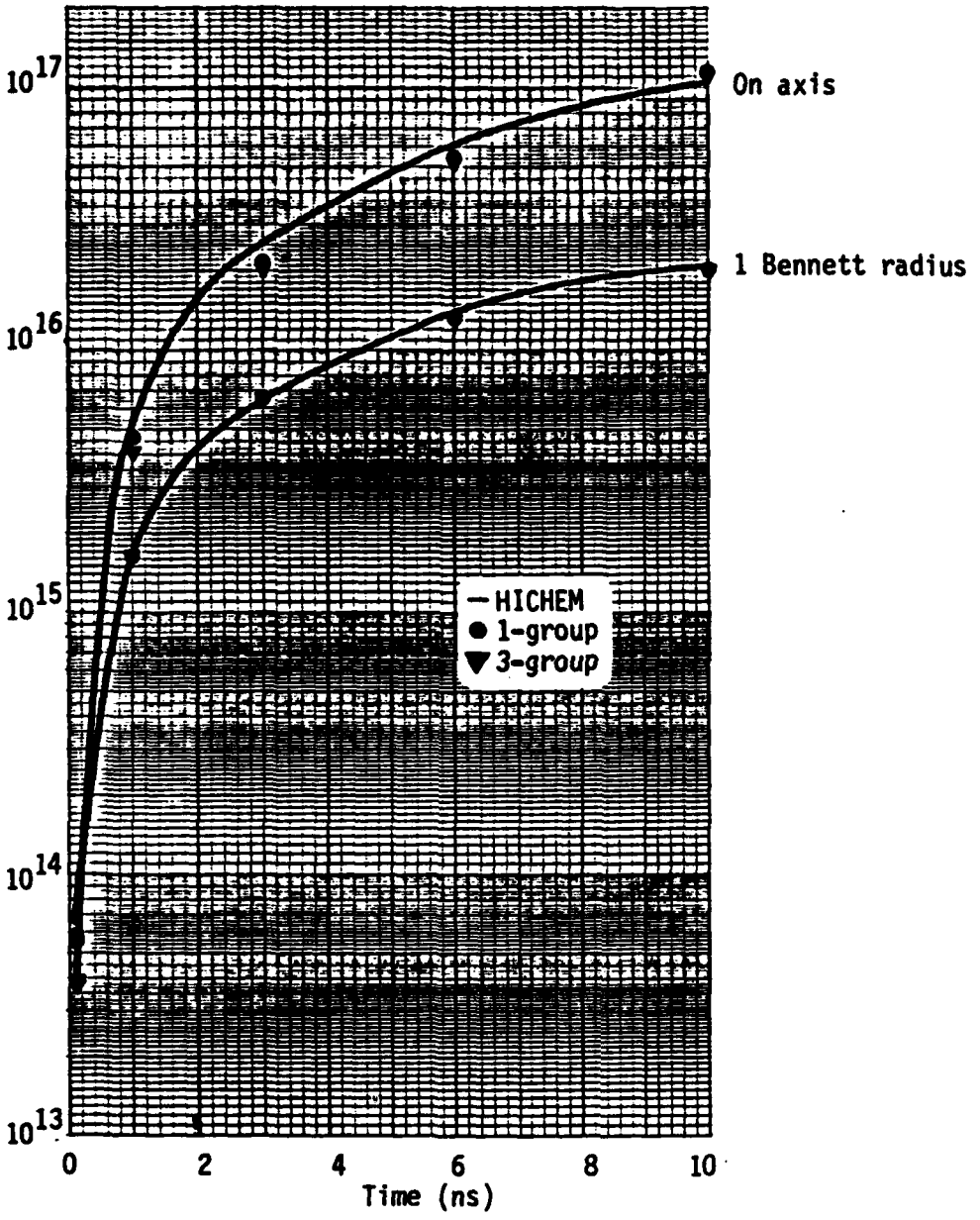

Figure 2.2. Electron Density Comparison at ρ/ρ_o = 0.1.

A similar comparison of electron temperatures and total currents is shown in Figure 2.3. The temperature agreement is quite good from 1 ns on. At 0.1 ns, HICHEM gives $T_e \sim 18$ volts, compared to the 12 or 13 volts given by the simple models. At such early times the ohmic approximation used in HICHEM is not very good, so the ohmic heating rate is likely to be incorrect; thus it is not clear which values are closer to the truth.

As in the 10 kA comparison (Ref. 1), the agreement between HICHEM and the simple models is not as good for the net current and effective current. This difference is mainly due to the difficulty in matching the momentum transfer frequency calculated in HICHEM by a very simple formula. However, the agreement in currents is still acceptable, particularly since the most interesting sensitivities described below (Section 2.5) develop before 1 ns.

Because the results of the HICHEM code are suspect below $\rho/\rho_0 \sim 0.1$, especially for $\xi <$ few ns, it cannot be used for calibration comparisons at lower densities. However, many of the results presented below are differential comparisons or sensitivity studies, and thus can provide useful information in spite of uncertainties in the quantitative results.

2.5 Computational Results

2.5.1 Introduction

The beam parameters for the calculations described below are:

Current	=	100 kA
Rise time	=	5 ns
Bennett radius	=	0.5 cm
Energy	=	10 MeV

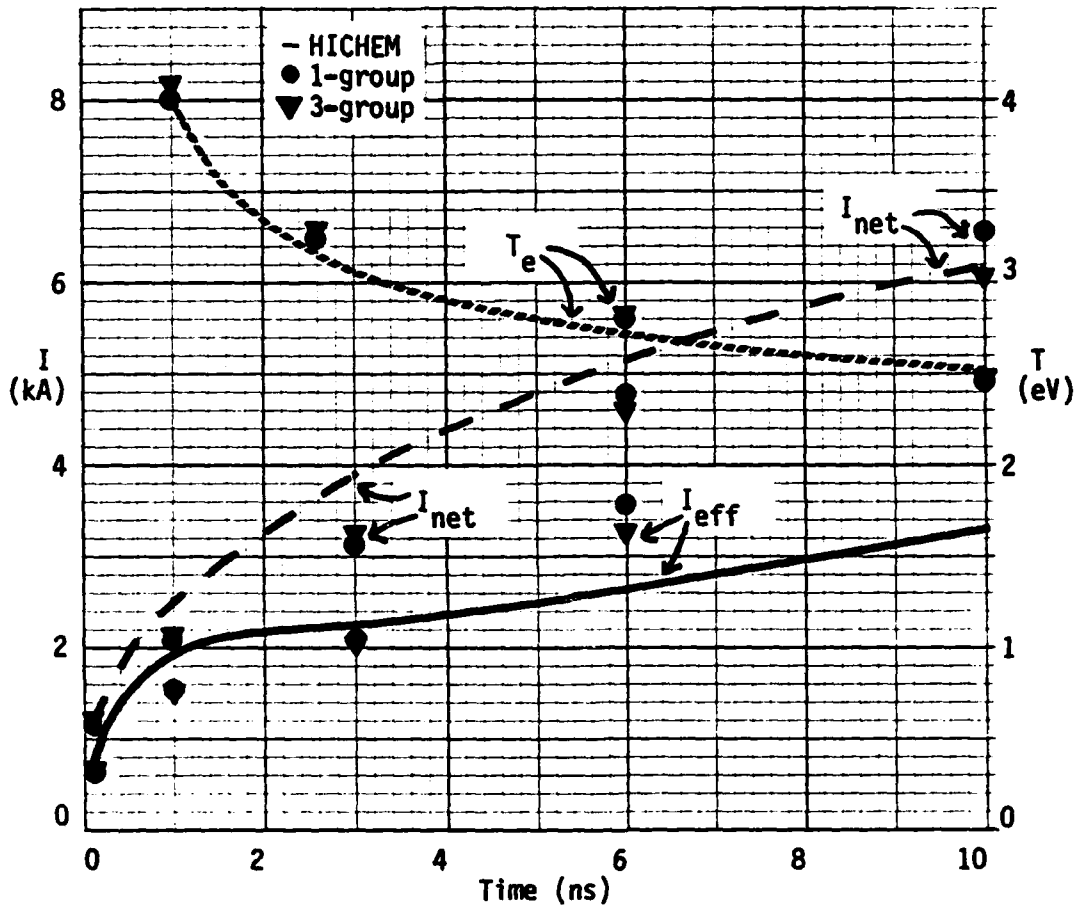

Figure 2.3. Axial Temperature and Current Comparison at ρ/ρ_o = 0.1.

The discussion below is divided into two main sections. The sensitivities to gas density, Hall currents, and pressure terms are described briefly in Section 2.5.2, and the remaining sections discuss the calculations in more detail.

The main conclusions have been stated earlier (Section 2.1). In brief, it has been found that the pinch force is strongly dependent on the gas density below some threshold value, and significantly dependent on the presence of Hall currents and pressure terms. The plasma current and electron density radial distributions change dramatically over a very small range of density ratio near $\rho/\rho_0 = .01$, resulting in an increase of pinch force by a factor of 3 or more for a density change of only $\sim$ 20%.

2.5.2 Sensitivity Results

2.5.2.1 Density Sensitivity of Pinch Force

The dependence of $I_{eff}(r)$ on ρ/ρ_0 is shown in Figure 2.4 for the three-group model, and in Figure 2.5 for the one-group model. The sharp onset of current enhancement begins in the range $\rho/\rho_0 \sim .0085 - .01$ for the three-group model, and between .005 - .008 for the one-group model. In both cases, the current enhancement is a factor $\sim$ 3.5 or greater, compared with a base level at $\rho/\rho_0 \sim .01$. These large effects set in when the plasma electrons can be sustained in a state of bulk runaway for several tenths of a nanosecond.

The sharp density threshold results from the sensitivity of the charge neutralization process to gas density. Several effects contribute. The beam production of positive ions is directly proportional to the density; the electrons produced by the beam provide "seeds" for the avalanche process of plasma electron collisions. The peak e-folding rate of the avalanche is also proportional to the density. These two processes clearly delay the charge neutralization as the gas density is decreased and allow higher radial electric fields to develop (assuming the rise time is not $\ll$ 1 ns). In order for

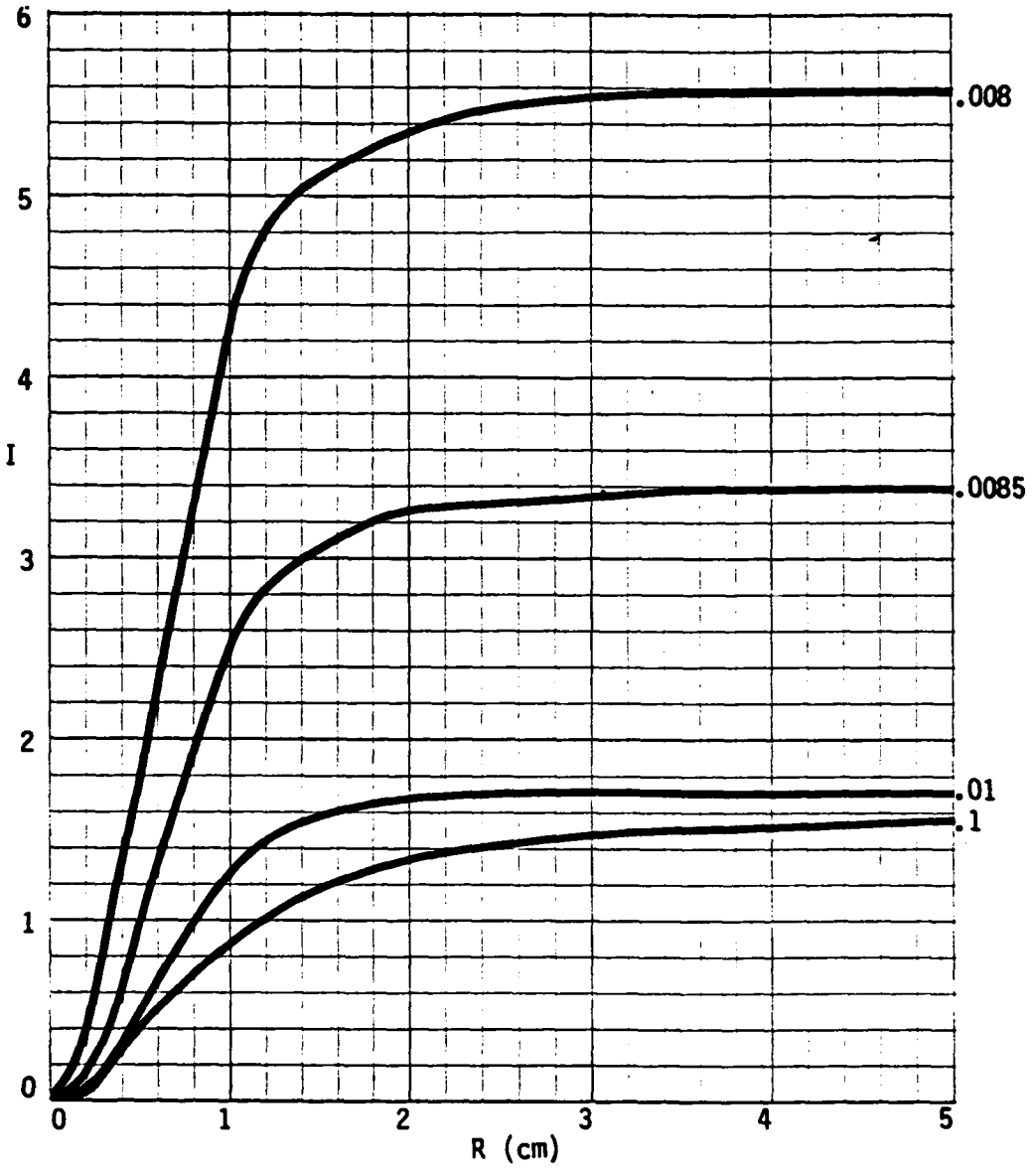

Figure 2.4. I_{eff} Dependence on ρ/ρ_0 at 1 ns (3-Group Model).

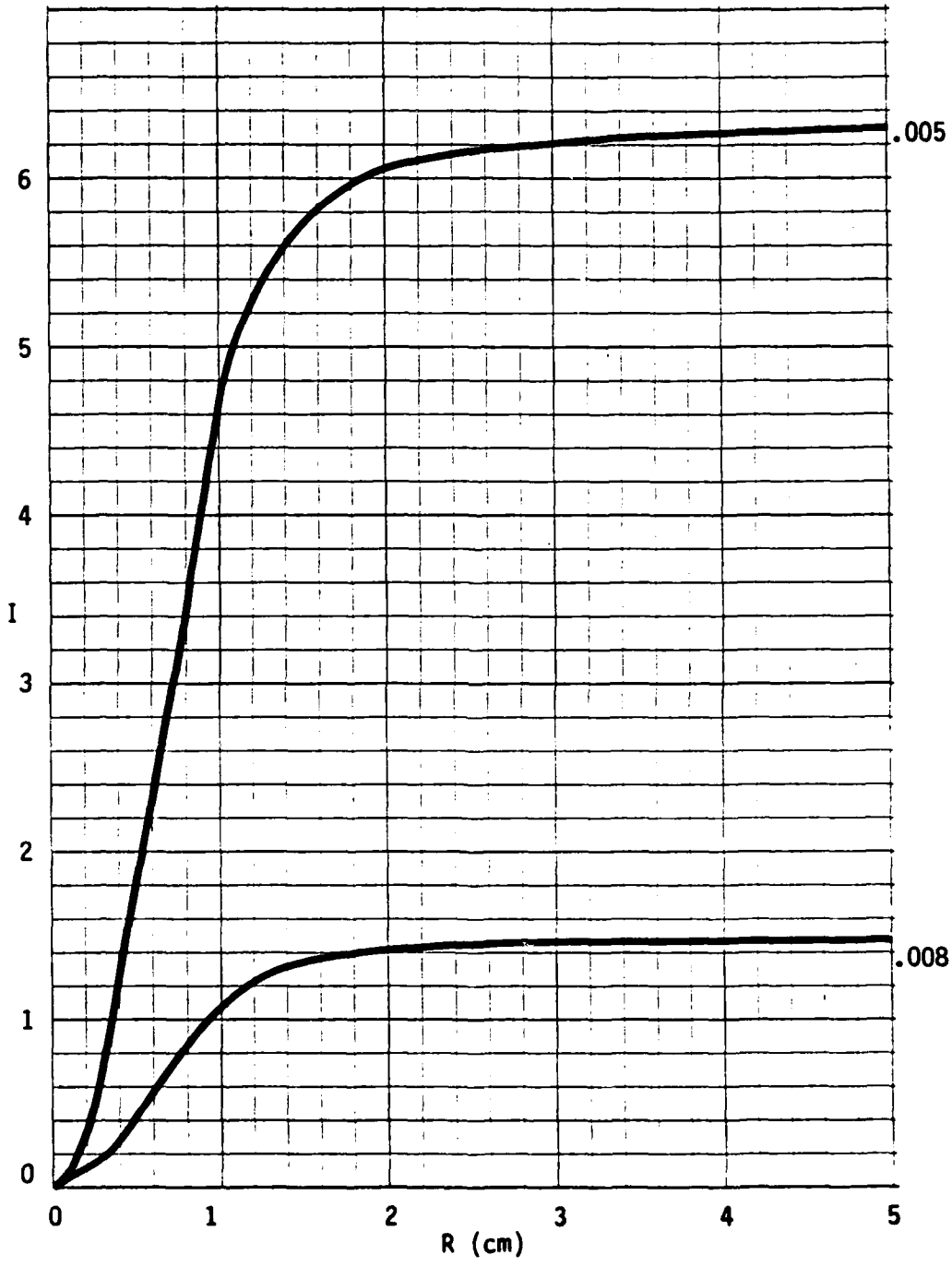

Figure 2.5. I_{eff} Dependence on ρ/ρ_o at 1 ns (1-Group Model).

neutralization to occur, plasma electrons produced by various processes must move out of the spatial region occupied by the beam, leaving the positive ions to cancel the charge of the beam particles. Higher fields help move the electrons out quickly, but that process dilutes very considerably the avalanche ionization and thus slows the production of the needed positive ions close to the beam axis. In the true IFR regime, avalanche is relatively unimportant, and the accumulation rate of beam-generated positive ions determines the neutralization time and the peak fields.

The difference in density threshold between the two models is caused by (1) the time-delay in ionization in the three-group model which reduces the effective beam ionization rate by more than a factor of two; and (2) the effects of the non-Maxwellian high-energy group on the ionization rate and on the movement of plasma electrons away from the beam. It is difficult to assess these separately because beam production of the high-energy and δ-ray groups (which degrade relatively slowly at low densities) is the cause of the time delay. Since qualitatively-similar results occur whether or not the high-energy group is included, it seems that the time-delay is probably most directly responsible.

2.5.2.2 Sensitivity to Hall Currents and Electron Pressure

The radial pressure gradient in the equations of motion for the high and low energy electrons can drive currents both radially and in the z-direction due to the magnetic part of the Lorentz force (Hall effect). This works in conjunction with the electrically driven currents. The result of deleting either the pressure terms or all Hall effects (by zeroing the magnetic force on the plasma electrons) is shown in Figure 2.6. Clearly, the Hall currents have the largest effect, but the pressure terms are not negligible either. Note that these comparisons show the cumulative effect of removing the terms for the entire calculation, and not simply the contributions to the current at the time shown. A similar calculation was done with only the high group

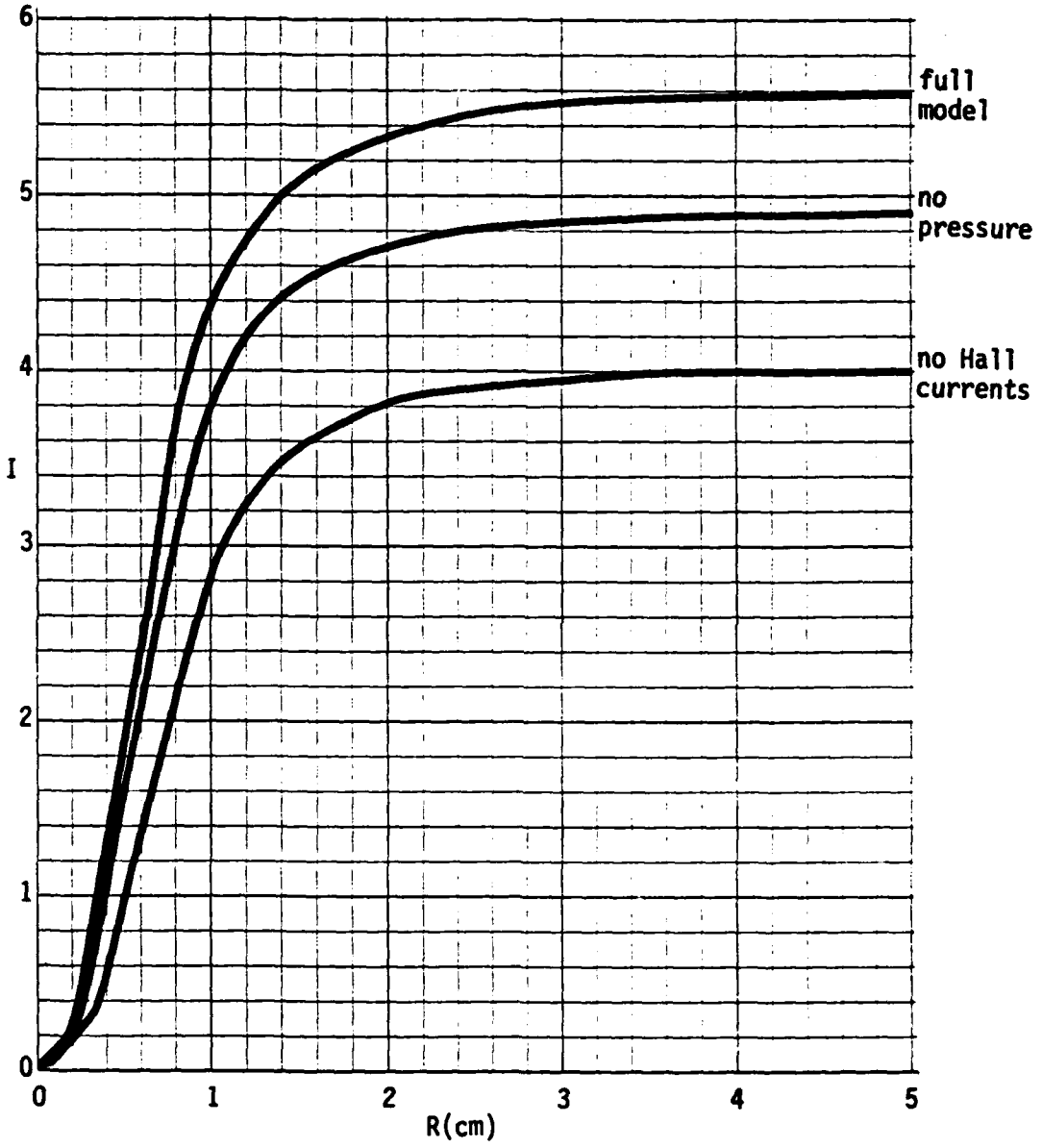

Figure 2.6. I_{eff} at 1 ns with ρ/ρ_o = .008 (3-Group Model).

pressure turned off. The effect at ξ = 1 ns was considerably smaller than shown in the figure. Low-group pressure contributes dominantly during the bulk runaway because the electrons reach temperatures in excess of a kilovolt, and their number density is large. However, it will be shown in later discussion that the high-group pressure-driven Hall current is important.

2.5.3 Comparison of 1-Group and 3-Group Calculations at ρ/ρ_0 = .008

The purpose of the following discussion is to provide a more detailed description of the phenomena which lead to the enhanced pinch force. At ρ/ρ_0 = .008, the 3-group model shows a very strong effect, whereas the 1-group model shows very little because its density threshold is somewhat lower.

2.5.3.1 Effects on Plasma Current Distribution

The net current (including displacement) integrated out to radius r is given by I_{net} = .005 r B(r), where I is in kA, B is in gauss, and r is in cm. The effective current, which measures the pinch force, is the beam-profile-weighted average of .01 r (B(r) - E_r(r)). The value of the effective current integral taken to radius r, and the net current, are shown in Figures 2.7(a) - (h) at various distances from the pulse head. Large differences are apparent by 1 ns and persist to 10 ns.

At 0.1 ns, the net currents for the two calculations are similar, but the effective current is substantially weaker for the 3-group case because the radial electric field is higher (due to slower charge neutralization).

At 1 ns the effective current in the 3-group model is $\sim$ 28% of the beam current at that time, whereas in the 1-group model it is only $\sim$ 7.5%. The net current profiles imply a very much broader plasma current distribution for the 3-group model, although net currents inside 5 cm radius (10 Bennett radii) are $\sim$ .5 to 1 kA in both cases even at 10 ns into the pulse where the beam current is almost 100 kA.

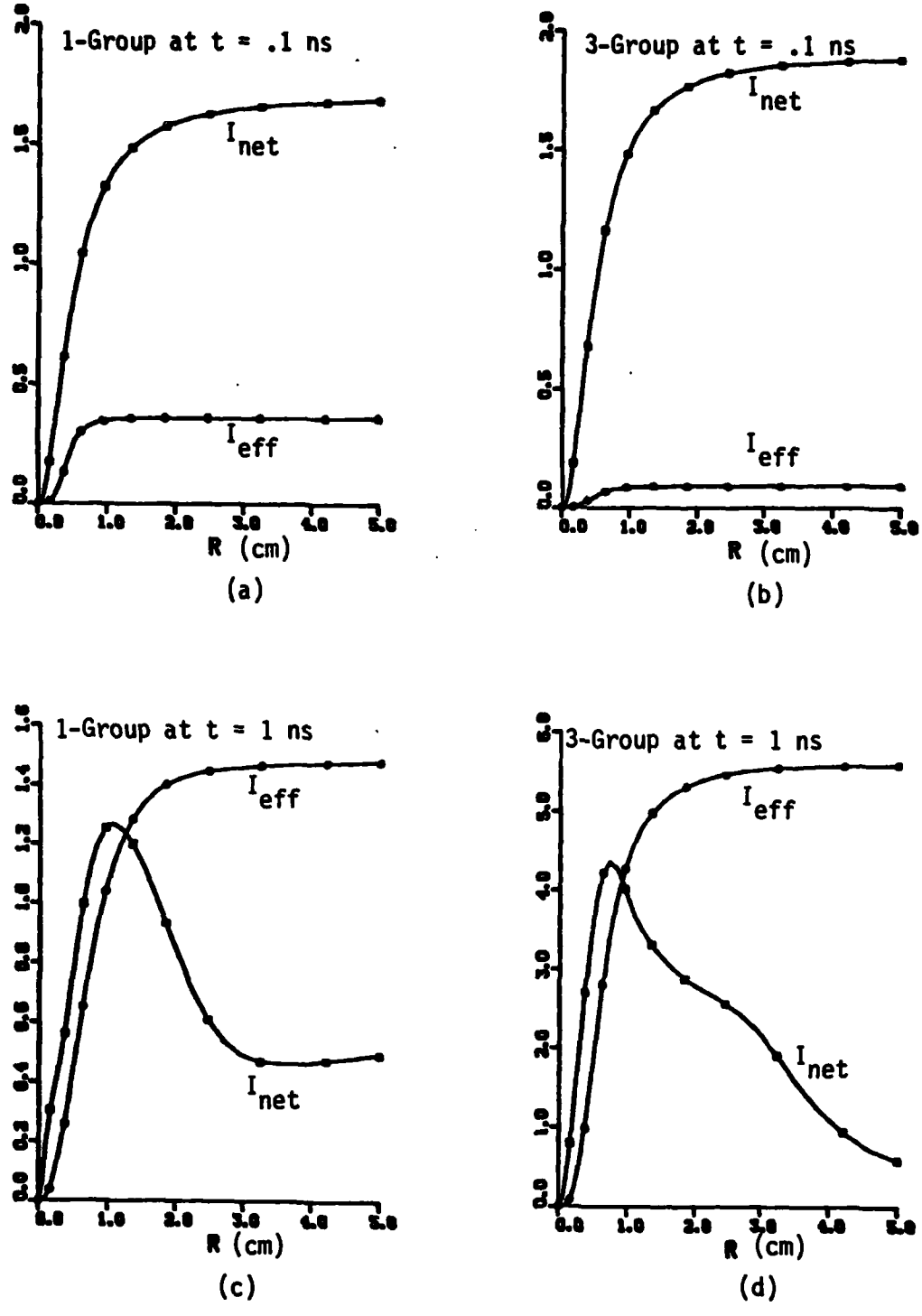

Figure 2.7(a)-(d). I_{net} and I_{eff} (ρ/ρ_0 = .008).

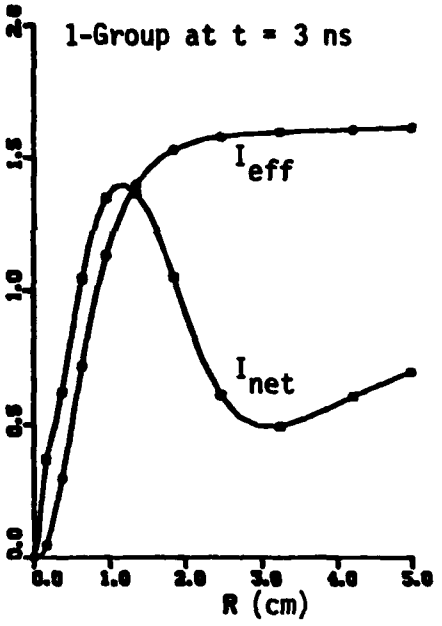

(e)

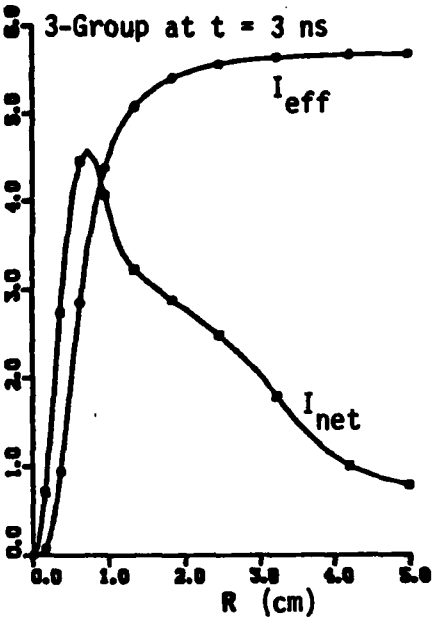

(f)

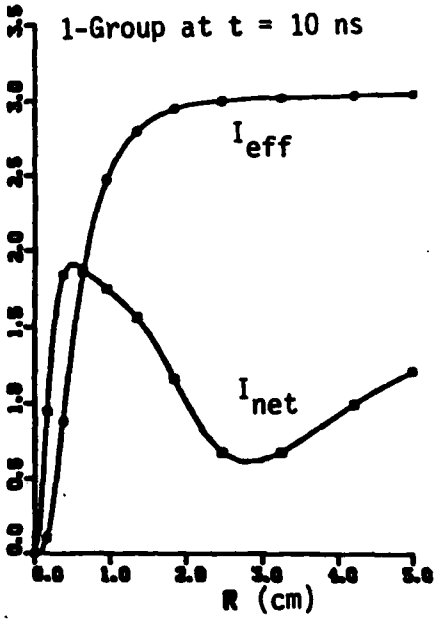

(g)

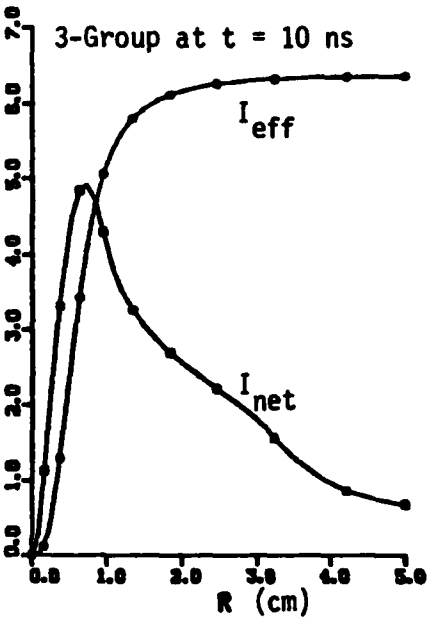

(h)

Figure 2.7(e)-(h). I_{net} and I_{eff} (ρ/ρ_o = .008).

A comparison of the plasma current (J_z) radial profiles at 1 ns is shown in Figure 2.8. The breakdown of the 3-group profile into contributions from the high and low-energy electron groups is discussed below in Section 2.5.4.4.

2.5.3.2 Electron and Ion Density Profiles

Major qualitative differences in the evolution of the electron density are apparent in Figures 2.9(a) - (d). The 1-group calculation shown in Figure 2.9(a) has the usual peak slightly off axis due to the E_r-initiated avalanche, and is not unusual. The 3-group calculation for the low group (Figure 2.9(b)) is much more interesting. It shows a large peak well off axis, and much higher density at large radius. The high-group density (Figure 2.9(c)) has features which invite interpretation as propagating sound waves. The ridge which appears earliest in time is associated with the rise of the E_r field, and the second begins on the axis near the peak of E_z. There is a hint of the first ridge in the low-group density also.

The total positive ion density is shown in Figure 2.9(d). Since the immobile ions show the same gross features as the low-group electron density, it is clear that the large off-axis peak must be interpreted in terms of the history of the ionization rates. However, the weak ridge in the low-group electron density does not appear in the ion density, and thus may be a flow feature. The number of particles in the high group is not large enough for the ridges of Figure 2.9(c) to show up in the ion density (Figure 2.9(d)). It seems likely that they are similar in nature to the ridge in the low-group electron density. Further support for the flow explanation is provided by Figures 2.10(a) and (b). These show the low-group and total ion-densities for the 1-group calculation at $\rho/\rho_0 = .005$, in which there is a large current enhancement compared to $\rho/\rho_0 = .008$ (see Figure 2.7). Here the ridge structures in the electron density are more prominent, but still have no strong counterpart in the ion density.

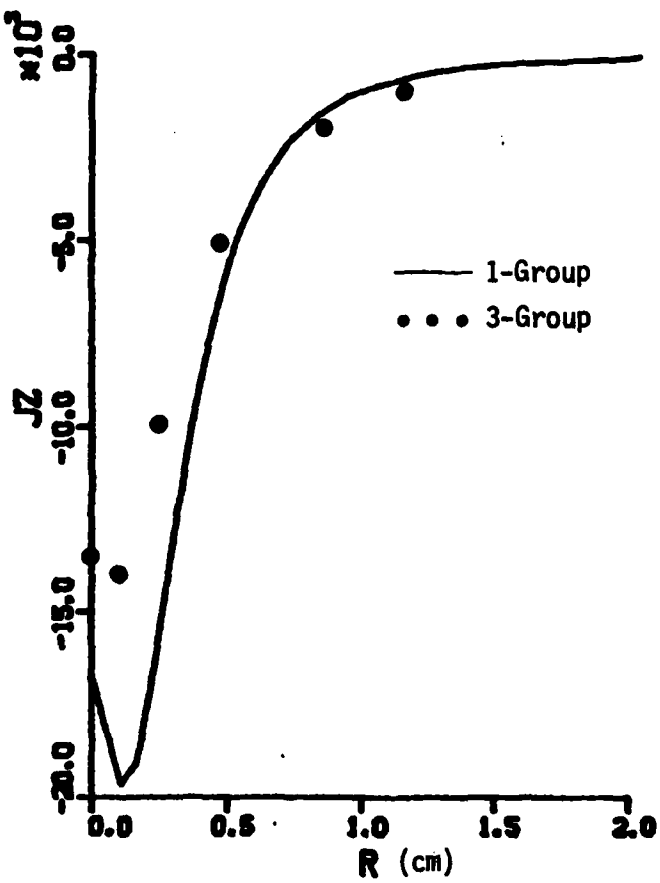

Figure 2.8. Plasma Current Density J_z at 1 ns (ρ/ρ_o = .008).

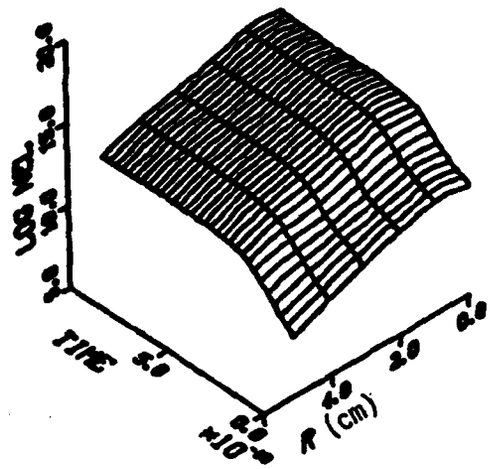

Fig. 2.9(a). Low Energy Group Electron Density (0-1 ns) for 1-Group Model at ρ/ρ_0 = .008.

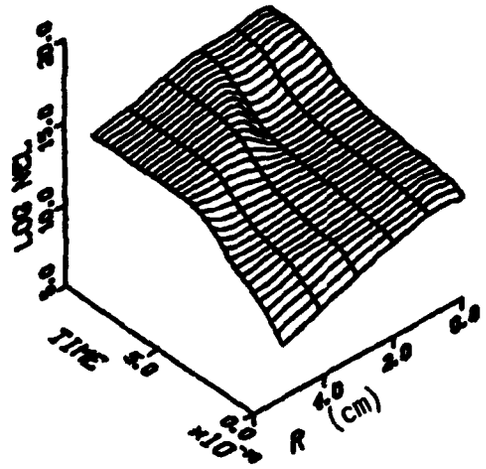

Fig. 2.9(b). Low Energy Group Electron Density (0-1 ns) for 3-Group Model at ρ/ρ_0 = .008.

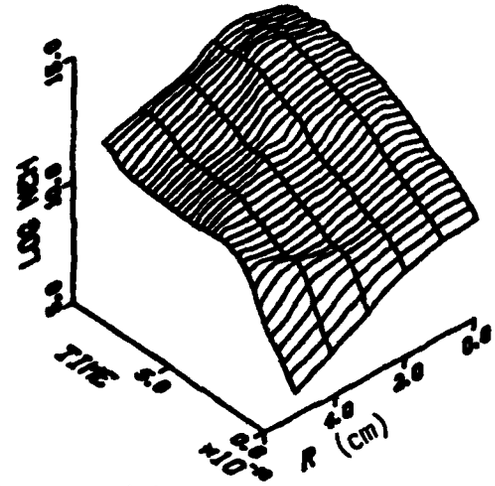

Fig. 2.9(c). High Energy Group Electron Density (0-1 ns) for 3-Group Model at ρ/ρ_0 = .008.

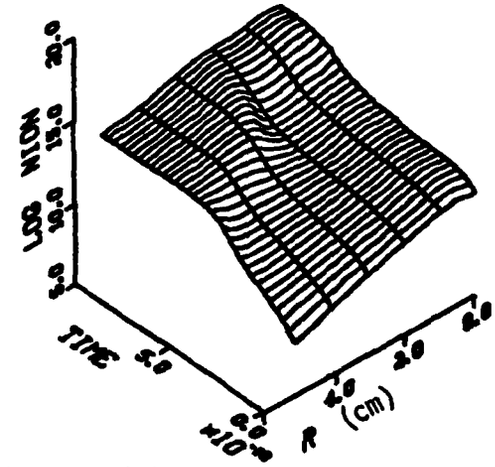

Fig. 2.9(d). Total Positive Ion Density (0-1 ns) for 3-Group Model at ρ/ρ_0 = .008.

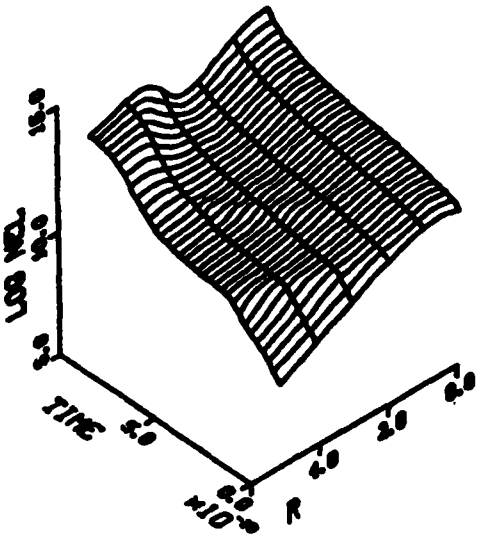

Figure 2.10(a). Electron Density (0-1 ns) for 1-Group Model at ρ/ρ_0 = .005.

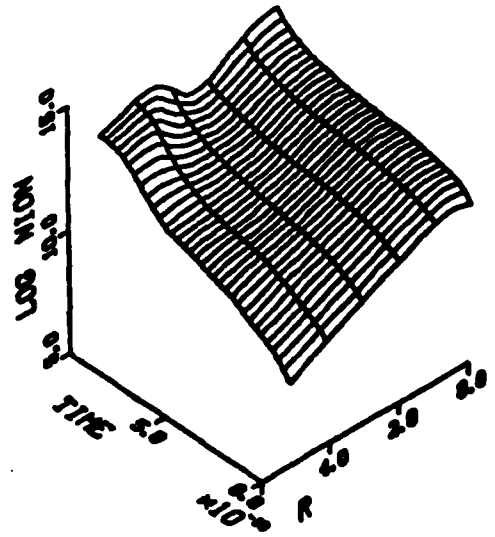

Figure 2.10(b). Positive Ion Density (0-1 ns) for 1-Group Model at ρ/ρ_0 = .005.

The difference in positive ion density radial profiles at 1 ns is shown clearly in Figure 2.11(a). At this time the ion density is much greater than the beam particle density, so these profiles are very close to the electron density in the charge-neutralized state. The effect on the z-component of plasma current was shown earlier (Figure 2.8). Figure 2.11(b) shows how the relatively small difference in ion densities on axis due to time delay before 0.1 ns, becomes very large for a few tenths of ns before coming together again.

For ease of detailed comparison, electron density radial profiles for the 1-group model, and for the low and high-energy components of the 3-group model, are shown in Figures 2.12(a) - (c). The large temporary off-axis hump in the low-group electrons is very clear at 0.6 ns in Figure 2.12(b). The very much broader density profiles produced by the 3-group model are also very obvious, and persist out to 10 ns from the pulse head.

A summary of electron and ion number density comparisons on axis is given in Table 2.1 below. The first two entries of the third column show the magnitude of the time-delay effect, while subsequent entries show the large differences seen in Figure 2.11(b). The first two columns give an indication of the importance of electron transport. At 0.3 ns for the 3-group model, only 47% of the plasma electrons ever produced on axis remain there.

TABLE 2.1

ELECTRON TRANSPORT EFFECTS

Time (ns)	(N_e/N_i) 1-Group	(N_e/N_i) 3-Group	$\frac{N_i(3\text{-Group})}{N_i(1\text{-Group})}$
.03	.98	.97	.69
.06	.87	.86	.68
.1	.77	.67	.37
.3	.99	.47	.014
.6	.99	.76	.027
1	.99	.99	1.27
3			.82
10			.93

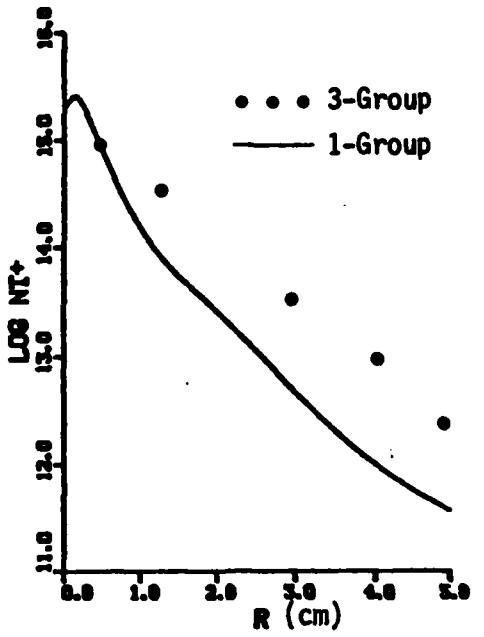

Figure 2.11(a). Positive Ion Radial Profile at 1 ns (ρ/ρ_0 = .008).

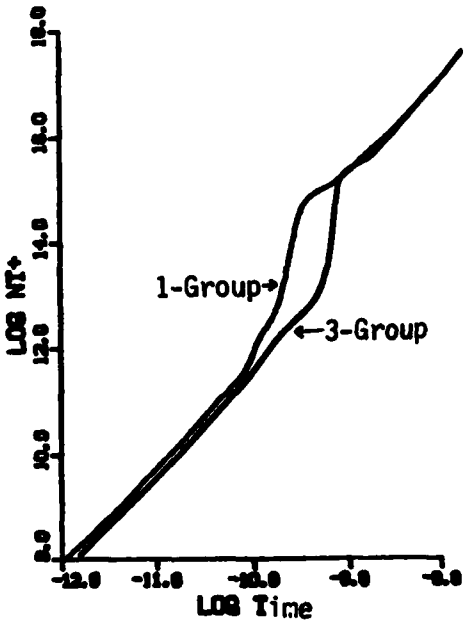

Figure 2.11(b). Positive Ion Density on Axis (ρ/ρ_0 = .008).

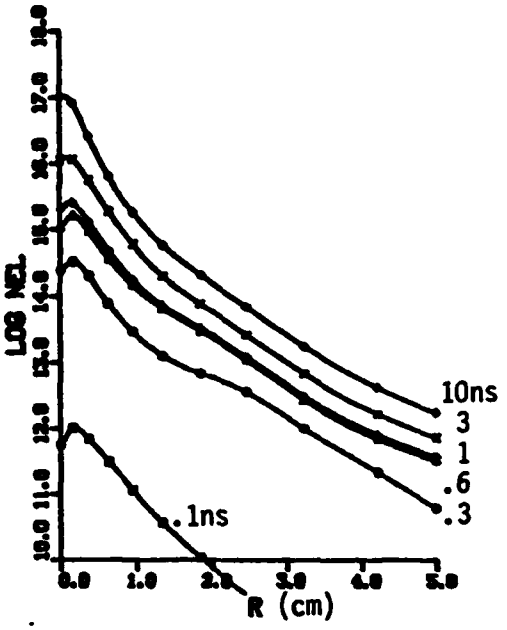

Fig. 2.12(a). Low Energy Group Electron Density Profiles, 1-Group Model (ρ/ρ_o = .008).

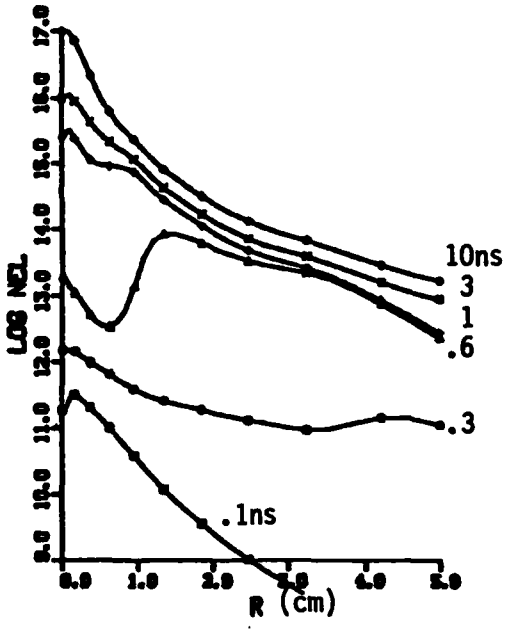

Fig. 2.12(b). Low Energy Group Electron Density Profiles, 3-Group Model (ρ/ρ_o = .008).

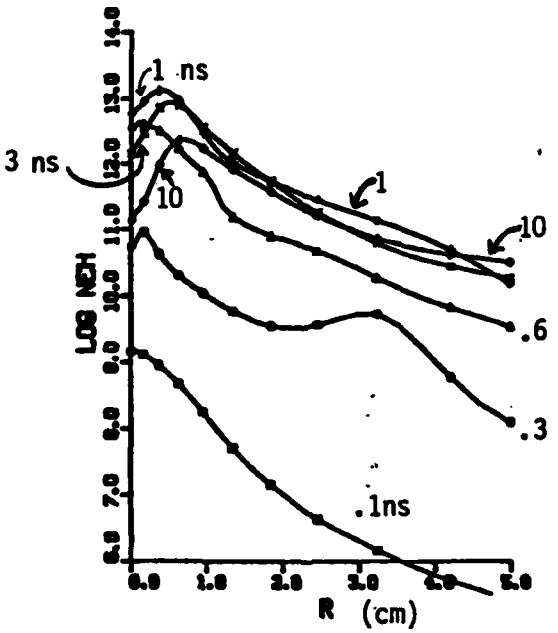

Fig. 2.12(c). High Energy Electron Density Profiles, 3-Group Model (ρ/ρ_o = .008).

2.5.3.3 Electric Field Effects

Both the E_z spike and the final decay of E_r occur significantly earlier in time for the 1-group model (Figures 2.13(a) - (d)), and the peak field strengths are lower. The large negative oscillation in E_r at 1 Bennett radius is especially prominent in the 3-group calculation, but appears to damp out satisfactorily. The negative spike in E_r in caused by an overshoot of the outward-moving electrons as charge neutralization is finally achieved near the axis. The significant overshoot is consistent with the fact that the electron plasma frequency is much greater than the collision frequency at $\sim$ 0.3 ns. The large off-axis hump in ion density at 0.6 ns (Figure 2.12(b)) seems to be associated with the deceleration of the low-group electrons by the reversed E_r, and by their final cooling through the peak of the ionization cross section. The final cooling occurs considerably earlier off-axis, as shown in Figure 2.14(a). The temperature behavior of the 1-group model is also shown for completeness in Figure 2.14(b).

2.5.4 Hall Current Effects

2.5.4.1 Introduction

Hall currents may be comparable to ordinary currents when the Larmor frequency eB/mc is comparable to or greater than the momentum transfer frequency. This criterion is a strong function of both ambient density and electron energy. The 3-group model allows the possibility of accounting for the energy dependence in a strongly non-Maxwellian plasma. The momentum transfer frequency at 1 eV in N_2 is about the same as that at 200 eV, and decreases with energy beyond 50 or 60 eV. Thus, if a substantial fraction of the electrons have energy in excess of 200 eV, their low momentum transfer frequency may result in a significant Hall current, out of proportion to their fractional number density.

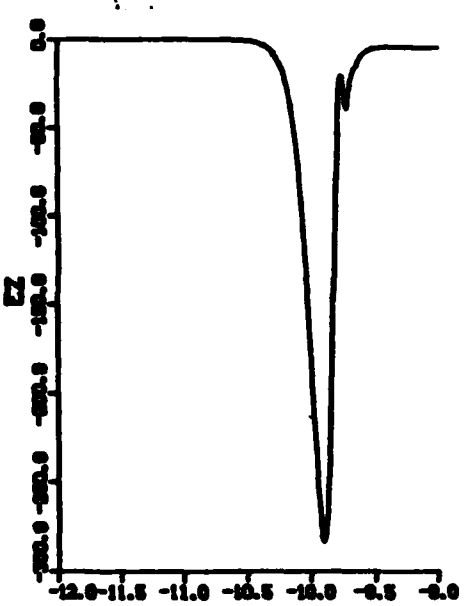

(a) 1-Group Model, On-Axis.

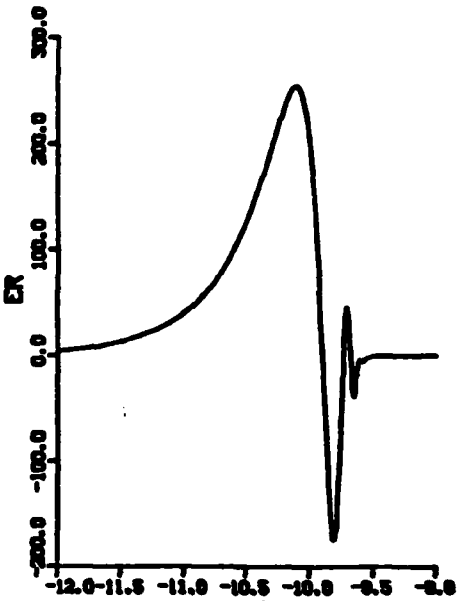

(b) 1-Group Model, 1 BR.

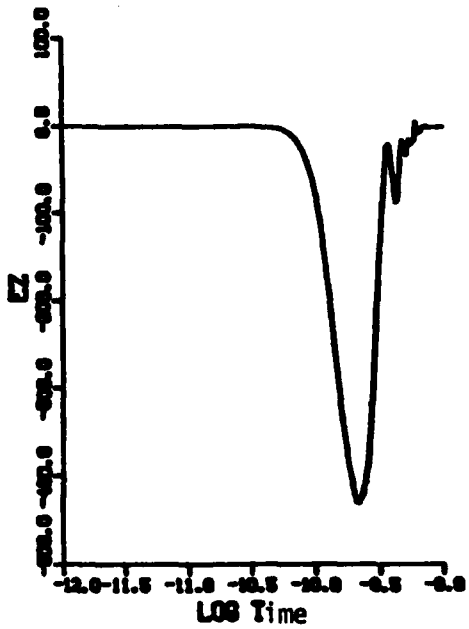

(c) 3-Group Model, On-Axis.

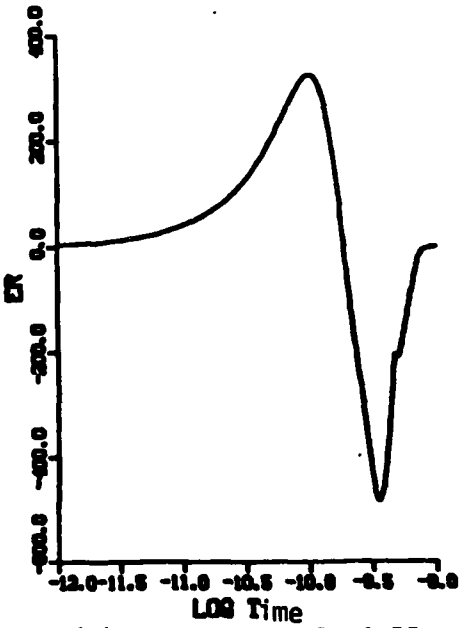

(d) 3-Group Model, 1 BR.

Figure 2.13(a)-(d). Electric Fields (ρ/ρ_o = .008).

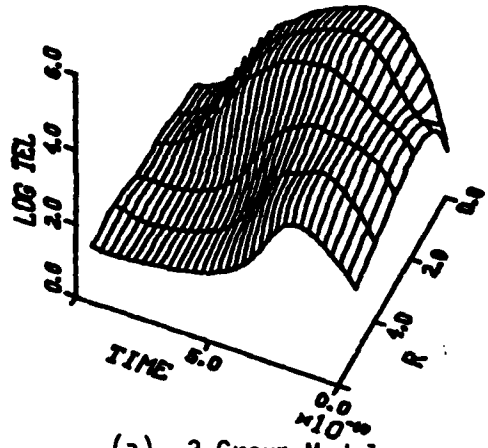

(a) 3-Group Model.

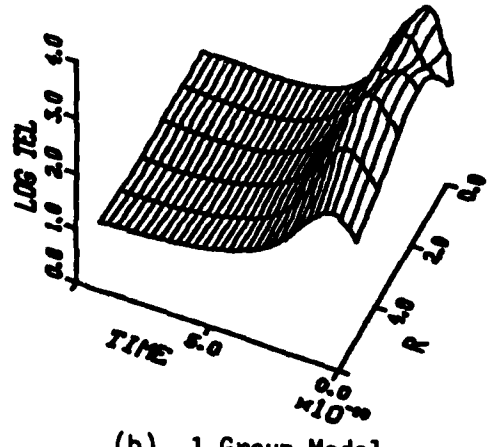

(b) 1-Group Model.

Figure 2.14(a) and (b). Electron Temperature (0-1 ns) ρ/ρ_0 = .008.

2.5.4.2 Detailed Discussion

It is clear from Figure 2.6 discussed in Section 2.3 above that Hall currents are important to the pinch force. In the calculation at $\rho/\rho_0 = .008$, even the low-energy electron group achieves high velocity for a short time, and contributes substantial Hall current. However, this is generally masked by the E_z-driven return current. In the far wings, however, and at early times near the axis, the radial outflow driven by E_r is turned forward by the magnetic field and the net plasma current density is forward. The amount of current involved, however, is insignificant in magnitude compared to the beam current.

When the high-energy electron group from the 3-group model is examined separately, it shows quite large effects. The z-component of plasma current for the high group is shown at various times in Figure 2.15(a). Beyond about 1.5 Bennett radii it is always directed forward with the beam. Nearer the axis. the strong E_z field keeps the current going backwards, although by 10 ns there is relatively little backward-moving current in the high group. A small part of this forward-going current is due to the fact that high-group electrons produced directly by the beam are injected with forward velocity. However, most of it is due to the Hall force acting on the radial out-flow.

The effect of Hall current in the high energy electron group is shown in Figure 2.15(b). At 1 ns, the forward-going current near 1 Bennett radius amount to almost 2 kA/cm^2, compared to the $\sim$ 5 kA/cm^2 of low group plasma current going backwards at the same radial position. The result is a very significant reduction of the total return current.

It is important to note that at late times $\xi \gtrsim 0.5$ ns, the radial flow which is turned forward by the magnetic field is driven not primarily by E_r, but by the radial pressure gradient of the high-group particles. Yu (Ref. 4) first recognized this as a possible important component of the total current.

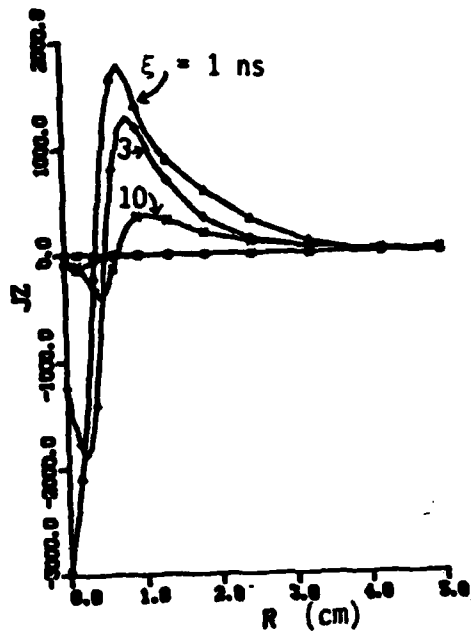

Figure 2.15(a). Current Density J_z of High Energy Electrons (ρ/ρ_0 = .008).

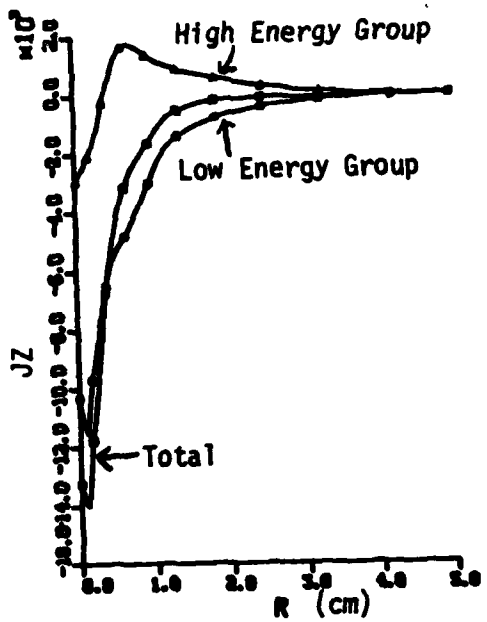

Figure 2.15(b). Effect of High Energy Electrons on Total Plasma Current Density J_z at 1 ns (ρ/ρ_0 = .008).

From the equation of motion it is clear that a density gradient is equivalent to a radial electric field of magnitude

$$E_r = - T \frac{\partial \ln N}{\partial r} \text{ volts/cm.}$$

For $T \sim 10$ KeV as suggested by Yu (and used for the high group in these calculations), and a density gradient with scale ~ 1 cm, this corresponds to $E_r \sim 10$ KeV/cm. Assuming that the system as a whole approaches a steady state solution of Maxwell's equations, J_r must $\rightarrow 0$. In the presence of the Hall-force terms, the radial E_r adjusts itself to shut off the net current driven by $v_z B_\theta$, E_r, and the pressure gradient. In the present context it seems that zero net radial current could perhaps be achieved by a balance between an inward flow of very low energy electrons and an outward flow of a much smaller number of fast electrons. Because of the differences in ν_m for the two streams, the corresponding Hall currents would not cancel exactly in this case. Under some conditions such counterflows may be limited by instabilities.

2.5.5 Delta Ray Effects at Low Density

Although the steady state δ-ray current is independent of air density, the time required for the current to reach its maximum value depends strongly on the density. There is also a significant dependence on the beam energy if only relativistic particles ($\gtrsim$ 1 MeV) are included, as shown in Figure 2.16. The pulse length used in this calculation was 100 ns. (A very steep drop in δ-current at 1 atmosphere on a timescale of 10 ns beginning just before the pulse ends is not shown.) It is clear that at densities as low as .01 atmosphere the δ-current represents a very small increment to the beam current over the first 10 ns considered in the calculations presented above. Before 0.1 ns, the δ-current is comparable to the plasma current in the z-direction, but both are very much smaller than the beam current. It seems unlikely that the relativistic part of the beam secondary cascade can be important at early times for air densities as low as .01 atomsphere. However, for propagation in a density channel, the interaction with the high-density walls may be very important.

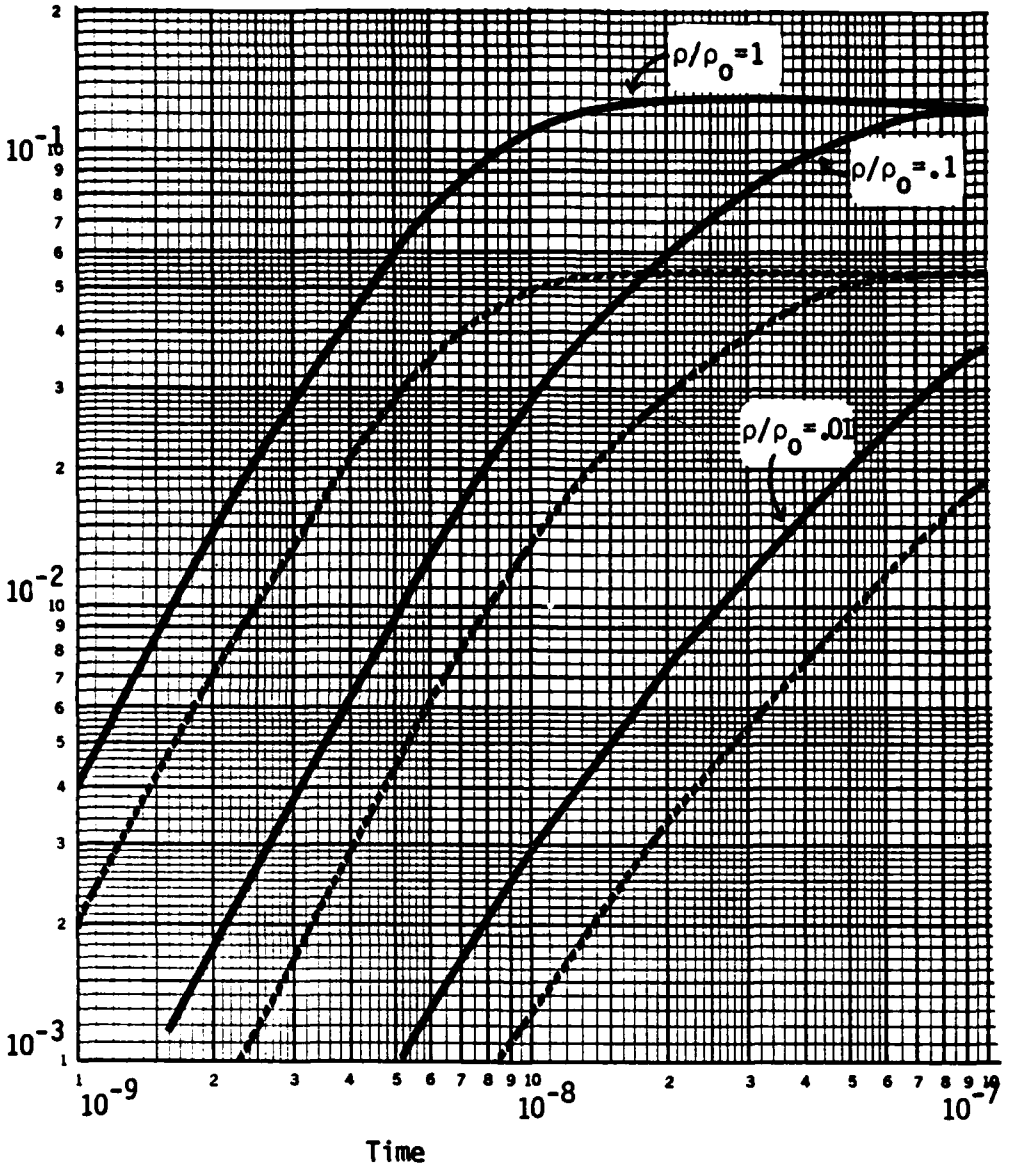

Figure 2.16. (Delta Ray Current)/(Beam Current) at Energy > 1 MeV.
Solid Curves: E_{beam} = 100 MeV
Dashed Curves: E_{beam} = 10 MeV

2.5.6 Comparison with Ohm's Law

Both the 1- and 3-group models use equations of motion to describe the electron flows. In general, the difference between the currents calculated this way, and by using an Ohm's law relationship involving only electron density and momentum transfer frequency, is large at early times. The duration of the deviation from Ohm's law decreases as the gas density decreases. Figures 2.17(a) and (b) show the actually-computed plasma current compared with what would have been obtained from an ohmic calculation using the instantaneous values of N_e and ν_m. The results are shown for the 1-group calculation at $\rho/\rho_0 = .008$, but comparable effects are present for the 3-group case. At 0.1 ns the ohmic current shows an extremely strong Hall effect due to the large radial field; the current given by the equation of motion is very much smaller, and the Hall effect does not show on the linear scale. At 1 ns, the two methods of calculating the current give virtually identical profiles, as shown in Figure 2.17(b).

2.5.7 Concluding Remarks

The calculations discussed above show the magnitude of the effects to be expected when low-density phenomena are taken into account. All the commonly used assumptions listed in Section 2.2 above have significant impact on the results at $\rho/\rho_0 = .01$. (The current carried by relativistic beam secondaries is important at low densities only if the pulse is long enough for the full build-up to occur.)

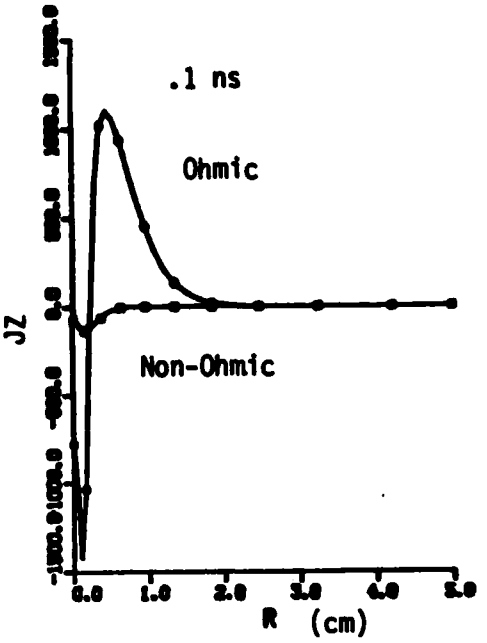

(a)

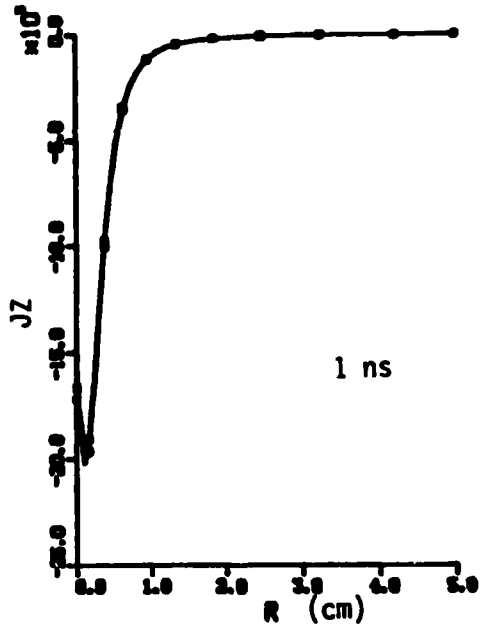

(b)

Figure 2.17(a) and (b). Comparison of Ohmic Calculation of Plasma Current Density with Equation of Motion Calculation.

3.0 HERMES HOSE EXPERIMENTS

During the period 01 September 1983 through 31 March 1983, SAI provided theoretical support to Sandia National Laboratory, Albuquerque (SNLA) to determine the relevance of the HERMES facility to address key uncertainties in high-current beam hose stability. The theoretical conclusion was quite optimistic: With proper pulse conditioning, and with small initial hose perturbations, hose growth should be small enough to permit adequate calibration of existing hose codes. Unfortunately, in the limited amount of time spent on the HERMES machine, it was not possible to solve all the difficulties associated with beam injection. Although the beam radius was small enough to be of interest (1-2 cm), the pulse was often injected off-axis (probably due to non-uniform cathode ignition). Various conditioning cells were employed with some success, but the initial hose disturbance was always too large to compare with low-amplitude, linearized hose models. Although theory predicts that hose should saturate after about 6 meters of propagation (with HERMES beam parameters), the measured hose displacements after only 50 cm of propagation were already in the non-linear regime.

It was noted by SNLA that in all drift chamber pressures a "low-frequency" hose sweep could always be detected (by the $\dot{B}_\theta$ probes and the Faraday cups) with frequencies between 30 and 70 MHz. This is in qualitative agreement with the high-frequency cut-off prediction of all multi-component hose models. At a fixed position z from the injection point, the dominant sweep frequency as the pulse passes should vary inversely with the magnitude of the instantaneous, magnetic-dipole relaxation time τ_d. The variation of τ_d with time, chamber pressure, and the distance z as predicted by the PHLAP code is in qualitative agreement with the observed variations in hose-sweep frequencies.

The SAI code PHLAP (Ref. 9) was employed to predict the hose growth of the HERMES pulse for various pressures and initial conditions. The beam current profile was taken directly from measured values and is plotted in Figure 3.1 as a function of time ξ (ns) at the fixed position $z = 0$. The retarded time

variable ξ measures the distance back from the pulse head. Although HERMES produces pulses with peak current greater than 100 kA, pulse conditioning reduces this to 40 kA. The beam energy is assumed to vary linearly from 3 MeV at $\xi = 0$ to 10 MeV at $\xi = 40$ ns and is held at 10 MeV for $\xi > 40$ ns. The initial emittance is chosen to match the pulse at $\xi = 35$ ns in air at 200 Torr with a Bennett radius of 3 cm.

In Figure 3.2, the displacement of the center of charge, 60 ns behind the head, is plotted as a function of propagation distance z. The initial dipole perturbation was random noise with a maximum amplitude of unity. (The PHLAP dipole model is completely linear.) The hose growth saturates at about $z = 6$ m with a maximum gain of 46 and then commences to damp-out.

In Figure 3.3, the maximum saturated gain is plotted for all positions behind the pulse head at two different propagation chamber pressures; 50 and 200 Torr. The saturation of maximum hose growth in the pulse tail is an important high-current prediction and hence, could in principle be tested with HERMES or other existing diode machines. In addition, the scaling of hose growth with pressure could also be calibrated in near term experiments.

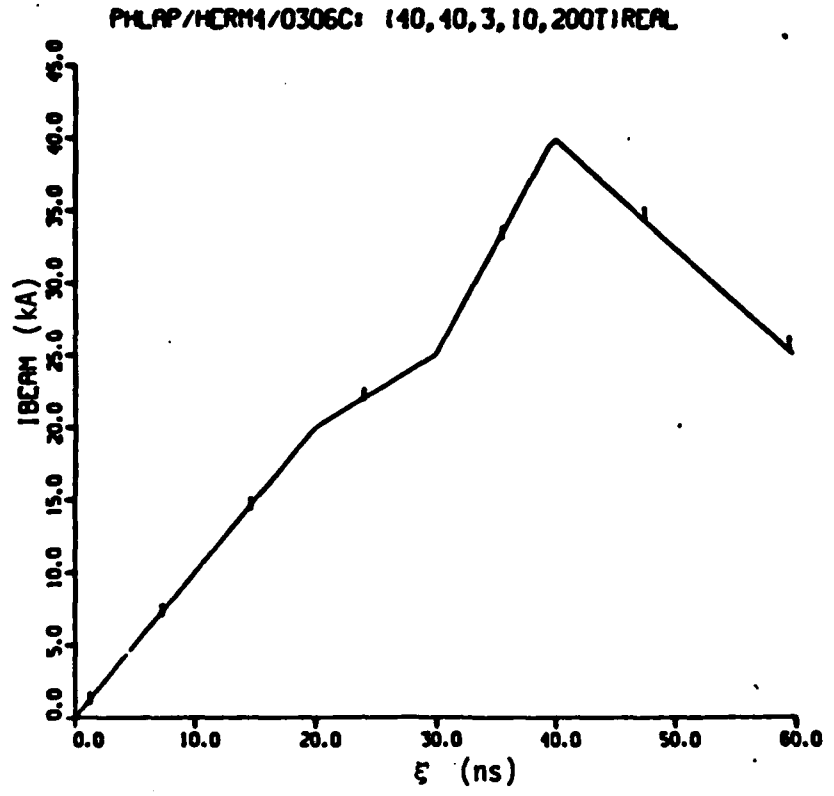

Figure 3.1 HERMES beam current at z = 0 as a function of time.

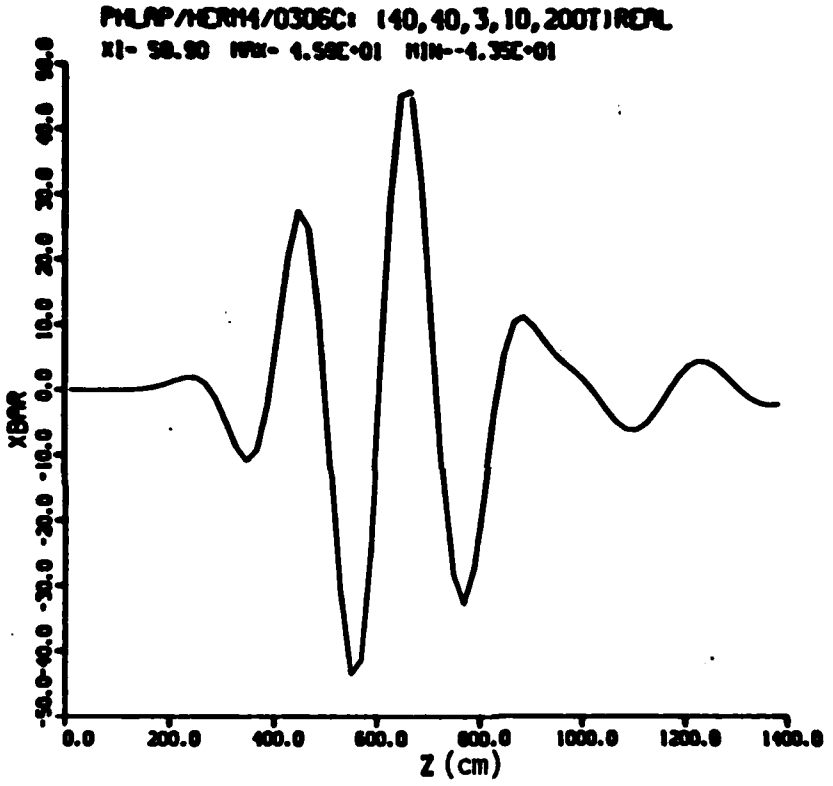

Figure 3.2 The displacement of the center of charge at ξ = 60 ns as a function of propagation range z.

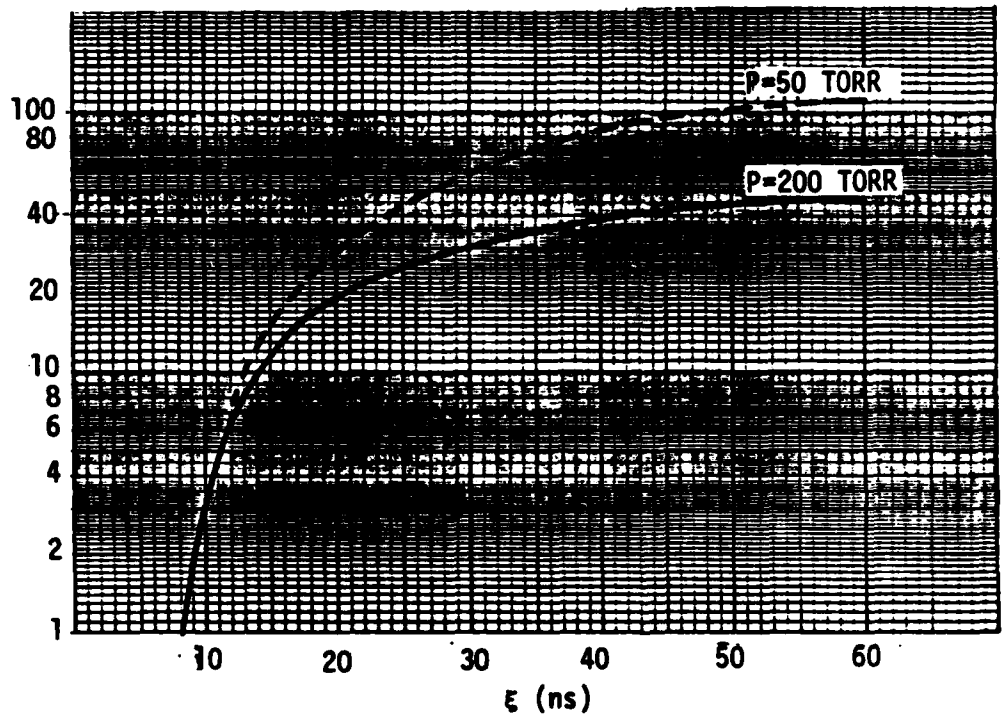

Figure 3.3 Maximum saturated hose growth

4.0 REFERENCES

1. "Consequences of Non-Ohmic Currents and Non-Local Energy Deposition for Electron Beam Propagation in Reduced-Density Air",D. A. Keeley and R. L. Feinstein, presented at the Fifth International Conference on High-Power Particle Beams in San Francisco, CA, 12-14 September 1983. (UNCL).

2. "Low-Density Conductivity Models" D. A. Keeley and C. L. Yee presented at the DARPA Propagation Review Meeting held in Monterey, CA, 20-23 June 1983 (UNCL).

3. "Studies in Hall Current Effects on Beam Propagation," R. R. Johnston, R. L. Feinstein, D. A. Keeley and H. R. Kirch, AFOSR Final Report, April 1982.

4. "Dynamics of Electron-Beam-Generated Plasma ... 100 TORR," S. S. Yu and R. E. Melendez (LLNL) presented at the APS Meeting, New Orleans, LA 05 November 1982.(UNCL).

5. "Studies in Beam Propagation Physics," R. R. Johnston and E. E. Simpson, SAI-C-38-PA, 9 August 1980 (SECRET).

6. "Modeling Beam Front Dynamics at Low Gas Pressures",R. S. Briggs and S. Yu (LLNL) 13 May 1982 (UNCL).

7. "Beam Conductivity Code HICHEM," D. A. Keeley, SAI-C-49-PA, 30 June 1981 (CONF).

8. "High Current Beam Propagation Studies: Theory and Experiment, and Sandia Final Report," R. L. Feinstein, D. A. Keeley, E. Cornet, W. Reinstra, SAI-C-56-PA, February 1983 (UNCL).

9. "Propagation Physics of High Current Beams, "R. L. Feinstein, D. A. Keeley, H. Kirch, and E. Simpson, SAI-C-42-PA, 23 October 1980 (SECRET).

END

FILMED

1-85

DTIC